Ordering and stability in lipid droplets with applications to low-density lipoproteins

Jarrett L. Lancaster, Todor Antonijevic, and Joseph M. Starobin
Department of Nanoscience, Joint School of Nanoscience and Nanoengineering, University of North Carolina at Greensboro, 2907 E. Lee Street, Greensboro, North Carolina 27401, USA
(Received 3 January 2014; revised manuscript received 29 April 2014; published 20 June 2014)

In this article, we present a framework for investigating the order-disorder transition in lipid droplets using the standard Ising model. While a single lipid droplet is itself a complex system whose constituent cholesteryl esters each possesses many degrees of freedom, we present justification for using this effective approach to isolate the underlying physics. It is argued that the behavior of the esters confined within lipid droplets is significantly different from that of a bulk system of similar esters, which is adequately described by continuum mean-field theory in the thermodynamic limit. When the droplet's shell is modeled as an elastic membrane, a simple picture emerges for a transition between two ordered phases within the core which is tuned by the strength of interactions between the esters. Triglyceride concentration is proposed as a variable which strongly influences the strength of interactions between cholesteryl esters within droplets. The possible relevance of this mechanism to the well known atherogenic nature of small low-density lipoprotein particles is discussed in detail.

DOI: 10.1103/PhysRevE.89.062708 PACS number(s): 87.10.Ca, 02.70.Uu, 05.70.Fh, 64.60.De

I. INTRODUCTION

In the thermodynamic limit, a vast array of tools [1,2] is available for studying phase transitions in numerous systems with different geometries and order parameters. Through renormalization group techniques, seemingly unrelated microscopic models can be shown to exhibit identical behavior near the critical temperature. For sufficiently large experimental systems, the results one obtains by taking the infinite, thermodynamic limit are often quite accurate. The power of the thermodynamic limit becomes somewhat muted when tackling small systems where the very notion of a true phase transition actually breaks down [3], as the finite-size effects and confinement can become important influences on the overall behavior [4].

The present work focuses on a class of systems known collectively as "lipid droplets" (LDs), which are organelles that form within eukaryotic cells as a means of lipid storage. The simplest picture of a lipid droplet is a mass of lipids surrounded by a phospholipid monolayer [5] with an overall spherical shape whose diameter can range from a few nanometers to well over a hundred micrometers [6]. In recent years a more complex picture of the various roles of lipid droplets within cells has emerged [7–12], indicating these structures may play an important role in processes as advanced as protein sequestration [13]. A complete description of their structure and interactions may be crucial to understanding obesity-induced insulin resistance [14] and liver disease [15]. An individual lipid droplet often contains a specific protein in its surface layer which is widely believed to strongly affect the specific interactions of the lipid droplet with its surrounding organelles [16]. This variety in specific proteins and enormous variation in size leads to a potentially overwhelming "zoo" of different LD particles. In this paper we present some results that should apply quite generally to generic lipid droplets, regardless of the particular protein embedded in the surface layer.

Though not commonly collected under the general umbrella of lipid droplets, low-density lipoproteins (LDLs) are particles of great physiological importance which consist of essentially the same ingredients; that is, masses of lipids surrounded by phospholipid monolayers with a specific protein residing in the surface of each particle. Apart from their rather prominent role [17] in the development of atherosclerosis, another reason LDL particles are often singled out from the general class of lipid droplets is their tiny size. The diameter of a typical LDL particle is about 22 nm [18], which makes it "invisible" to the traditional biochemical methods, such as density-gradient centrifugation, used to isolate larger lipid droplets [19]. Of interest to the present work is the fact that LDL particles are known to exhibit a type of order-disorder phase transition within their lipid cores which occurs at a critical temperature roughly equal to biological temperature [20,21]. It is unknown if this transition is physiologically important, but as we demonstrate, this transition should be a generic feature of lipid droplets. Additionally, there is even debate regarding the precise nature of the lipid ordering when the LDL particle is below the critical temperature, and evidence for several ordered core structures has been proposed [22–24]. Recent molecular dynamics studies [25] have highlighted the complex structure of the core lipids at biological temperature and found evidence for strong interactions between the lipids inside the particles and proteins embedded in the surface layer. The approach in this work will be somewhat "coarse-grained" as our focus will be on the nature of the order-disorder transition within a general lipid droplet. The relevance of our findings to understanding the specific structure and dynamics of LDL particles will be discussed.

With such a gap in the literature regarding theoretical investigations of the core dynamics in LD particles, the aim of the present work is to make a first step toward modeling the behavior inside these particles which captures some of the physics relevant to the dynamics of LDL particles. We demonstrate that an Ising model with static defects is able to capture several known experimental results concerning the nature of the phase transition when varying levels of triglycerides are present. These preliminary results allow us to examine the stability of two types of ordering within the low-temperature phase, which hints at possible directions

for future investigations into the atherogenic nature of the smaller and denser subsets of LDL particles. Furthermore, our approach does not rely on any specific property of LDL particles, so our results should be relevant to the properties of generic lipid droplets, which are currently of great interest in several biomedical fields [10,13–15,26]

The organization of this paper is as follows: in Sec. II we introduce the details of lipid droplets, including relevant properties of LDLs, which will be important for our analysis. We also discuss some important experimental results and the conclusions drawn from them regarding the core structure in LDL particles, as well as what is known about the order-disorder transition that takes place within the core of lipid droplets near biological temperature. In Sec. III we present the Ising model as a means for studying the lipid-droplet physics that mean-field theory in the thermodynamic limit is incapable of describing. Section IV contains our analysis of the stability of various ordered phases within the core and a sketch of possible connections of our results to the known dangerous nature of smaller LDL particles [27]. Finally, we conclude in Sec. V.

II. LD AND LDL BACKGROUND

At the simplest level, LD particles are packages for neutral lipid storage found in all types of eukaryotic cells, from mammalian tissue to yeast cells [28–30]. Enormous variation exists in size [5,19] and lipid composition [28,31], and the presence of particular proteins is believed to be related to the specific function of a given droplet [13,16]. Indeed, it has only recently been appreciated that LD particles serve important purposes in cellular function beyond the simple storage of fat [32]. Many interesting questions concerning the mobilization and release of fats are largely unexplored [33], and studies are just beginning to reveal valuable information about the internal structure of these droplets by employing methods such as freeze-fracture electron microscopy [34]. It appears that structure within the lipid core depends strongly on the lipid composition of the core [19,35], as a lack of structure appears highly correlated with the presence of "defects" which dilute the interactions between rod-like esters which exhibit a tendency to align at low temperatures [36]. Freeze-fracture immunocytochemistry has provided evidence [37] for a concentric-shell structure of the lipid droplet cores, though how such ordering forms has not been established. With such wide variation in lipid droplet composition and structure, our main interest will lie in results which do not depend on the microscopic details of the particular droplet but only on the coarse-grained picture of the lipid droplet's composition.

As an example of a particular particle which fits under the umbrella of lipid droplets, we briefly discuss the microscopic details of LDL particles, which are of great interest for their role in the development of heart disease. LDL particles are spherical nanoparticles with an average diameter of 22 nm. The outer shell of LDL consists of an apolipoprotein B-100 (ApoB100), phospholipids, and free cholesterol [18]. The core of LDL particles contains cholesteryl esters (CE), triglycerides (TG) and some cholesterol (FC). The ApoB100 protein makes up approximately 20% of the particle weight, and the rest of the weight comes from lipids. Of the total amount of lipids, 56% are CE, while the largest minority of the remaining mass consists of TG [20]. The calorimetric [21,38] and x-ray scattering [22,39] experiments performed on LDL samples reveal that a reversible transition from smectic liquid crystal to isotropic liquid occurs within the core CE in the temperature range from 20 °C to 45 °C. Based on recent findings [22,35,40,41], CE in the core are able to form layered structures. The details of the observed phase transition naturally depend on the particular composition and structure of a given LDL particle's core. Extensive experimental research [42,43] has revealed LDL particles to be composed of distinct subspecies, each with different sizes and compositions. Most notably, the relative number ratio of CE/TG molecules varies from less than 2 to greater than 10 [42]. The effects of the mass ratio of CE/TG has long been investigated with respect to the nature of the phase transition [23] as well as with respect to physiological implications. Indeed, in the case of monkeys, this ratio was shown to be strongly affected by diet, and an increased level of TG appears to broaden the phase transition [44], as well as to lower the transition temperature [23,45]. Many other factors, for example gender [46] and exercise [47], have also been shown to affect the specific lipid composition within an individual's LDL population. Interestingly, it has also been shown [36] that an apparently identical transition occurs within larger lipid droplets contained yeast cells, which suggests a sort of universal nature to this phase transition. The universality of this phase transition with respect to different types of lipid droplets and the apparent importance of the CE/TG ratio to its nature leads us to explore a two-component picture of the core's composition in which the dominant constituent is CE, and a small amount of TG is incorporated as "defects" which make no contribution to the interaction energy between two nearby lipids. Thus, in what follows we make no reference to the particular details of LDLs or any other specific LDs, focusing instead on general results which may be predicted from this coarse-grained approach.

In a larger sense, there is great interest in the structure and dynamics of the smaller variety of LDL particles, which are known to be more atherogenic than their larger counterparts [27]. The scientific reason for this is not known, and it is quite possible that an abundance of smaller LDL particles is itself not a danger but a harmless byproduct of some other more damaging risk factor. This puzzle has led to significant research aimed at finding the root of atherogenicity in certain classes of LDL particles as well as examining the reactivity of various constituents found within LDL particles [48]. There appears to be evidence for smaller, denser LDL particles being linked to high levels of TG in the bloodstream [49], and atherogenicity has been linked to the details of the ApoB100 protein's binding affinity [50]. By studying general lipid droplets we make no claims of a complete description of an actual LDL particle, as we are neglecting many of the realistic complexities of a real LDL particle; most notably, the presence of the ApoB100 protein. However, to the extent that the interations with the surface can be incorporated into our approach, we will show agreement of our findings with the results a more detailed microscopic description [25]. Thus, the goal of the present work is to isolate the mechanism responsible for the observed order-disorder transition using as few physical ingredients as possible.

III. ISING-LIKE APPROACH

A. Ising model

A seemingly natural starting point for a description of the cholesteryl esters within lipid droplets is provided by the mean-field theory presented by McMillan [51]. Applying this methodology to the present problem is straightforward. McMillan's model extends the basic Maier-Saupe theory [52] by taking into account both smectic-A and nematic ordering by the use of two order parameters. Except in extreme cases, the theory predicts two phase transitions separating the the smectic and nematic phases and the nematic and isotropic phases. Based on general estimates for the geometry of cholesteryl esters [53], McMillan's mean-field theory seems to predict two phase transitions instead of a single one, when applied to the core CE within lipid droplets. It is worth noting that McMillan's mean-field theory applies to a bulk mass of liquid crystals, infinite in extent. One generally finds that, in dealing with a finite number of particles [1] when confinement of the system is present [4], divergences and discontinuities are smoothed out to some extent. Thus, by taking into account these complications, it is expected that this pair of sharp transitions would be blurred out into a smooth "bump," which describes an effective phase transition between the ordered (smectic) and disordered (isotropic) phases, as is observed in experiments with LDL particles [22]. As we shall demonstrate, the phase transition is nothing special to LDL and should be a generic feature of lipid droplets.

To investigate the nature of the order-disorder transition within lipid droplets, we will employ the classical Ising model [1,2,54], described by the following Hamiltonian,

$$H_{\text{Ising}} = -J \sum_{\langle \mathbf{i},\mathbf{j} \rangle} s_{\mathbf{i}} s_{\mathbf{j}} - h \sum_{\mathbf{i}} s_{\mathbf{i}}, \tag{1}$$

where the variables $s_{\mathbf{i}}$ are "spins" living on a lattice of any dimensions and taking values ± 1. $-J$ is the energy associated with a bond between aligned spins. In one dimension there is no phase transition at nonzero temperatures, and in two dimensions with zero magnetic field ($h = 0$) the model is exactly solvable in the sense that one may derive a closed-form expression for the free energy [55]. In the two-dimensional model, a phase transition occurs at $k_B T_c = 2J/\ln[1+\sqrt{2}]$, where $k_B \approx 8.62 \times 10^{-5}$ eV/K is Boltzmann's constant. The approximate heat capacity neat the critical point is given by [54]

$$\frac{C(T)}{N k_B} \approx -\frac{2}{\pi}\left(\frac{2J}{k_B T_c}\right)^2 \ln\left|1 - \frac{T}{T_c}\right| + \text{const.} \tag{2}$$

The phase transition is second order in nature, as the free energy itself is a continuous function of temperature. In three dimensions, a similar phase transition occurs, but the model is no longer exactly solvable. Furthermore, the introduction of a magnetic field renders the two-dimensional model analytically intractable. While often used as a simplified model for ferromagnetism, the Ising model is special in that it is essentially the simplest classical system exhibiting a phase transition at a nonzero critical temperature. For this reason, the Ising model is often employed as a first step toward modeling much more fundamentally complex systems, from chemical kinetics to social dynamics [56]. In this work, we use the Ising model as a means to describe the order-disorder transition that takes place within lipid droplets.

B. Ising model applied to lipid droplets

As our main focus is on applications to LDL, we will model lipid droplets with comparable size to LDL particles. A typical LDL particle contains roughly 1000–1500 individual esters [18,42], and we can imagine a crude mapping between the core CE within a lipid droplet and a two-level system. Specifically, we wish to model a single layer within a smectic-ordered core as a two-state system in which each ester is in one of two states ($\xi_{\mathbf{i}} = 0,1$), so that the effective Hamiltonian describing the system is

$$H = -\epsilon \sum_{\mathbf{i}} \xi_{\mathbf{i}} - \tilde{J} \sum_{\langle \mathbf{i},\mathbf{j} \rangle} \xi_{\mathbf{i}} \xi_{\mathbf{j}}, \tag{3}$$

where ϵ is the energy difference between the two states and an interaction energy $-\tilde{J}$ is associated with two neighboring esters in which each is in the $\xi = 1$ state. The mapping $s_{\mathbf{i}} = 2(\xi_{\mathbf{i}} - \frac{1}{2})$ transforms Eq. (3) into the Ising Hamiltonian in Eq. (1) up to an irrelevant constant with

$$\tilde{J} = 4J, \tag{4}$$

$$\epsilon = 2(h - 4J), \tag{5}$$

for the two-dimensional model with four nearest-neighbors for each spin. In what follows, we will employ the "spin language" for simplicity and work with $h = 0$ to reduce the number of free parameters. Strictly speaking, this choice sets the energy of the $\xi = 1$ state *above* that of the $\xi = 0$ (i.e., $\epsilon < 0$). The $h = 0$ limit was also employed in Ref. [57] to investigate the properties of the melting transition in saturated triglycerides. In a similar spirit, our approach will be to use this limit to make the model as simple as possible so that the effects of introducing defects discussed in Sec. III C may be seen as clearly as possible. Within a single layer, the tail configuration of a single cholesteryl ester is labeled by a pseudospin $s_{\mathbf{i}} = \pm 1$. The configuration corresponding to frozen smectic order is assigned $s_{\mathbf{i}} = +1$, and a two-level approximation is employed to map any other configuration to pseudospin $s_{\mathbf{i}} = -1$, as shown in Fig. 1. Mapping the esters to pseudospins is simply a standard reduction to a two-level system [57,58], and the terminology should not be taken literally. Clearly, this model is too simple to capture many of the detailed predictions from a more sophisticated theory. The merit of using the Ising model lies in the simplicity of the model, and we take this approach as a way to make general statements about systems exhibiting effective order-disorder transitions, such as the core CE within lipid droplets. A lattice version of Maier-Saupe mean-field theory known as the Lebwohl-Lasher model [59] is another pseudospin approach to modeling liquid-crystal systems in which the pseudospin variables directly correspond to the director order parameter field of the liquid crystal. For purposes of this work we find the crude two-level Ising model quite adequate.

For comparison to experiments, we may consider a total Hamiltonian consisting of an Ising-like piece describing

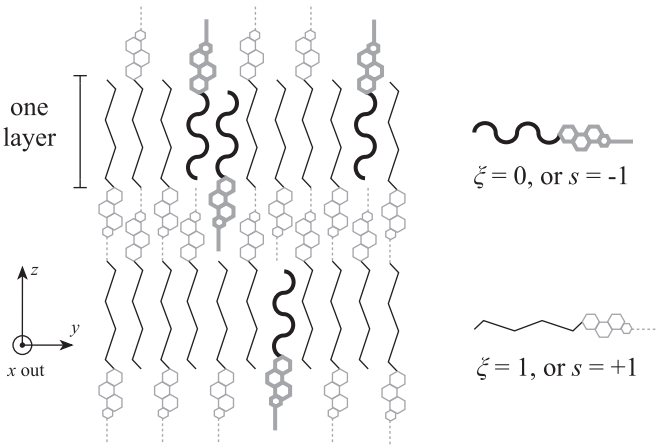

FIG. 1. Two-state approximation for the configurations of individual cholesteryl esters within a lipid droplet. The coarse-grained states of the esters are labeled in the spin language by s_i and in the lattice gas language by ξ_i. We consider a single two-dimensional sheet in the xy plane.

interactions and a phenomenological, bulk piece which only depends on temperature,

$$H_{\text{total}} = H_{\text{Ising}} + H_{\text{background}} \tag{6}$$

$$= -J \sum_{\langle \mathbf{i},\mathbf{j} \rangle} s_\mathbf{i} s_\mathbf{j} + \gamma N k_B T + \frac{\eta}{2} N k_B T^2. \tag{7}$$

The temperature-dependent terms merely serve to provide a constant shift and background linear trend to the specific heat curve,

$$C(T) = \frac{\partial}{\partial T} \langle H_{\text{total}} \rangle \tag{8}$$

$$= \gamma N k_B + \eta N k_B T + \frac{\partial}{\partial T} \langle H_{\text{Ising}} \rangle, \tag{9}$$

which provides a framework consistent with experimental results [20–23]. There is no predictive power in this addition. Rather, this provides a way to fit the "background" piece of the experimental specific heat curve so that it may be subtracted from the total signal, yielding the so-called "excess" specific heat [4], which we model using the Ising model with temperature-independent exchange interaction energy J.

In the thermodynamic limit, the choice of boundary conditions does not affect observables. Loosely speaking, one would expect the effects of the boundary conditions to vanish as the system size is increased, but it is not clear if a single LDL-sized lipid droplet is "large enough" to not require a careful treatment of the boundary. To fix the system, let us specialize to two spatial dimensions with periodic boundary conditions in what follows. While the physics will clearly depend strongly on dimensionality, our motivation for choosing two spatial dimensions is as follows: recent experiments [22,35,40] provide strong evidence that layered structures of CE form within the ordered phase inside LDL particles. These layers are essentially two-dimensional sheets in which the esters would only feel weak interactions with esters from other layers. Neglecting for a moment the spherical confinement favored by the protein shell, we are left with essentially independent layers which act effectively as two-dimensional, uncoupled subsystems. The choice of periodic boundary conditions is merely for convenience and this choice has no effect on the results of this work. Furthermore, this choice of periodic boundary conditions is not meant to imply these results are applicable to the infinite system periodic boundary conditions are often used to mimic. A discussion of how the effects of the lipid-surface interactions can be incorporated into this model via a different choice in boundary conditions is discussed in Sec. III D.

C. Triglycerides as defects

With this apparatus in hand, we will use it in this subsection to model an observed feature of LDL particles. Until this point, we have proposed the Ising model to describe the degrees of freedom related to ordering of cholesteryl esters within lipid droplet cores with no mention of the other agents present. The most notable agent also found in lipid droplet cores, as well as within LDL particles, is a significant concentration of triglycerides (TG) [42,43], whose direct interaction with cholesteryl esters is assumed weak compared to the ester-ester interactions. Thus, to a first approximation, one may consider the triglycerides within the Ising language as "defects," in which the spin is set to zero instead of ± 1, representing a cell with no contribution to the interaction energy.

In has been observed [23] that a critical mass ratio of esters to triglycerides of roughly CE:TG = 7:1 separates two qualitatively different classes of LDL particles. For larger concentrations of triglycerides, the critical temperature decreases with increasing TG concentration, whereas for smaller TG concentrations the critical temperature is somewhat insensitive to TG concentration. The original experiment showed that the critical temperature still does decrease with increasing TG concentration, but at a significantly reduced rate, so that a single line cannot be used to fit all the data. The original interpretation [18,23] of this result was in terms of a microphase separation between the CE and TG constituents for sufficiently high CE:TG ratios: for high CE:TG, the TG would be concentrated in the inner core, sufficiently separated from the CE so that a change in concentration has little direct effect on the CE in the outer core. Above this critical ratio, the CE are not sufficient in number to completely surround the TG, and the excess TG coexist with CE, so that adding even more TG to the core dilutes the CE, significantly altering their tendency to order and suppressing the critical temperature. In light of recent evidence for a lamellar structure within the core [22,35,40], there has been no revised explanation for the existence of this critical concentration within LDL particles.

As a first step toward exploring the effect of nonzero triglyceride concentration within the framework of the Ising model, we randomly fix a set number of lattice sites to zero and simulate the system's behavior, computing the specific heat as a function of temperature at various concentrations of these defect cells. We then repeat this computation by taking the same fractional area of the system as defect cells, but within a localized region. A graphical depiction of these arrangements is shown in Fig. 2. For computations, we chose a system of 20×20 spins, and the details of our simulations

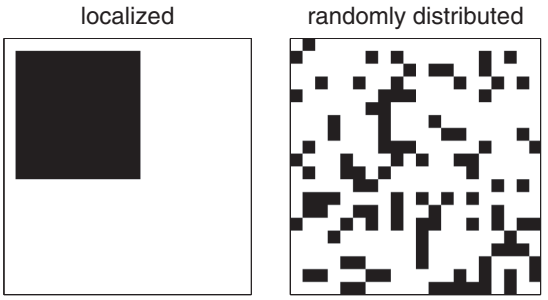

FIG. 2. Example of random defect distribution (right) and localized defect distribution (left). Defect cells representing TG molecules (value 0) are shown in black, while working cells representing CE molecules are shown in white. Here $n_d/n = 0.25$, where n_d is the number of defects and n is the size of the lattice leaving $n^2 - n_d$ CE molecules.

are discussed in Appendix A. The results are shown in Figures 3–4 and demonstrate that the critical temperature only depends on defect concentration when these defects are distributed throughout the entire system volume and not localized to the inner core of the lipid droplet in a manner that mimics the predicted microphase separation. Shown in these figures are results for $n_d/N = 0,0.1,0.25$ where n_d is the number of defect cells and n is the size of the square lattice so the number of sites is $N = n^2$. This means that the actual number of cholesteryl esters which is needed for normalizing the specific heat is $N - n_d$, and not simply n^2.

These results provide rigorous justification for the following simple picture: for randomly distributed defects, the effective interaction energy should decrease monotonically with increasing defect concentration as depicted in Fig. 4. Since $T_c \sim J$ by dimensional analysis, one sees that the critical temperature should also decrease monotonically with no critical concentration occurring. However, for localized concentrations of defects, we are effectively considering smaller systems with a new boundary at the interface between the fluctuating spins and the defect cells. As the defect concentration is increased, this boundary simply grows in size

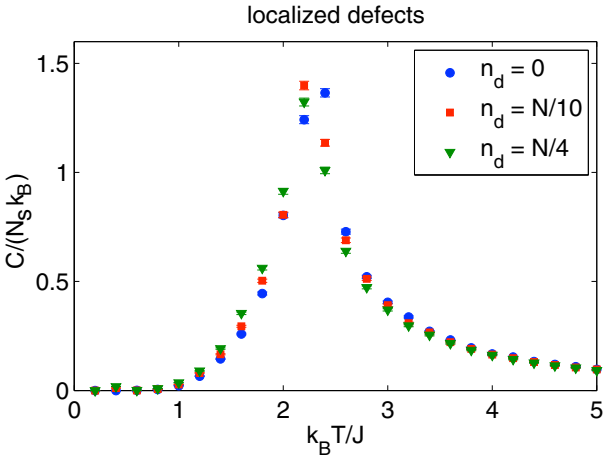

FIG. 3. (Color online) The nature of the phase transition is essentially unchanged as the number of localized defects is increased.

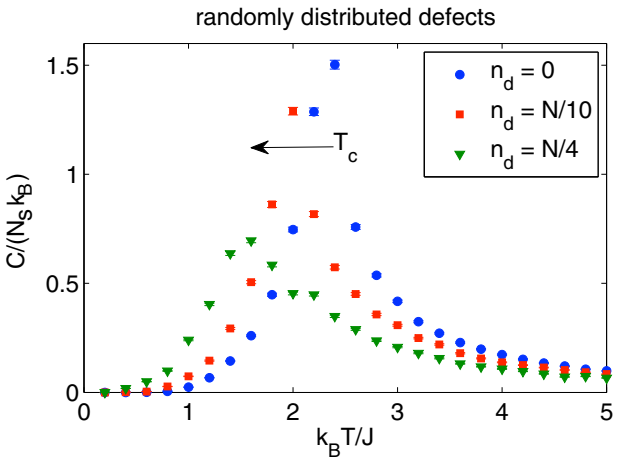

FIG. 4. (Color online) With random defects, the amplitude of the specific heat decreases as more defects are added. The critical temperature is also reduced as more defects are added.

as fewer spins are allowed to fluctuate. In the thermodynamic limit, this has no effect on the critical temperature, and so Fig. 3 demonstrates that in our finite system we find only a very weak dependence of T_c on defect concentration as should be expected from general reasoning. Figure 3 is really a demonstration that, despite the finite size of the system in question, we are in some sense "close enough" to the thermodynamic limit for such reasoning to apply.

Regularly spaced defects within the Ising model have been investigated extensively [60], and several analytic results in particular situations are available. Interestingly, the phase transition remains second-order in nature, though with renormalized critical exponents, for regularly spaced defects. However, any small amount of randomness in defect distribution is sufficient to change the transition to weakly first-order in nature [61]. Additionally, it is known in Ising systems that the transition temperature should decrease monotonically with increasing dilution and ultimately approach zero at some sort of percolation threshold [62,63]. It should be noted that many of the results in these references arise from the use of "frozen spin" defects instead of our "dead cells," in which the value of zero is assigned to a defect. A frozen spin is a site whose value is fixed at ± 1. Admittedly, this approach provides no possible mechanism for a crossover between these two regimes as the defects are fixed in space.

An interesting question would be whether allowing defects a dynamical degree of freedom—-that is, allowing these defects to move during the Metropolis sampling—would create such a crossover. It is quite clear from energy considerations that the localized configuration of defects results in a lower energy of the system at low temperatures than a random distribution of defects, since the localized configuration minimizes the number of broken bonds in the system. Preliminary simulations, involving an additional step in the Metropolis sampling in which a defect cell may be swapped with a "live" spin with some acceptance probability, appear to confirm that the localized configuration of defects does represent the true equilibrium state of the system at low temperatures. However, investigating this mechanism for defect arrangement in any

detail is beyond the scope of the present work. The main result of this section is justification of the proposition [23] for microphase separation when the transition temperature does not depend strongly on the triglyceride concentration.

D. Interactions at the surface

In this subsection, we demonstrate that the results presented above are not dependent on choice of boundary conditions. It is well known [54] that the effects of a particular choice in boundary conditions should vanish in the thermodynamic limit, but, with a system as small as those considered above, the particular choice of boundary conditions could have considerable effects on the dynamics of the system. By considering a circular domain with the spins on the boundary fixed $s_{\mathbf{i}} = 1$, we demonstrate that (1) the results of this explicitly finite-sized system are insensitive to particular choice of boundary conditions and that (2) within the framework of this model the expected effects [25] of interactions of the bulk lipids with the ApoB100 protein and phospholipids at the surface do not qualitatively change the nature of the phase transition. That is, the phase transition survives this perturbation, and the critical temperature decreases as the defect concentration is increased in a manner similar to the system with periodic boundary conditions.

To demonstrate points (1) and (2), let us now consider a square lattice of $n \times n$ points, where the spins are allowed to fluctuate within the subdomain $\mathcal{D}$, where

$$\mathcal{D} \equiv \left\{ \mathbf{i} = (i_x, i_y) \middle| \left(i_x - \frac{n_+}{2}\right)^2 + \left(i_y - \frac{n_+}{2}\right)^2 < \left(\frac{n_-}{2}\right)^2 \right\}, \tag{10}$$

where $n_\pm = n \pm 1$. For spins outside of this circular domain, we fix $s_{\mathbf{i}} = +1$. In what follows we set $n = 25$, so that the number of "live" spins is 437. Because the interactions are only between nearest neighbors, the only frozen spins which affect the system are those along the nearly circular boundary which encloses the dynamical part of the system. Molecular dynamics calculations have shown [25] that one prominent effect attributable to the boundary is a tendency to order among cholesterol esters close to either the ApoB100 protein or the phospholipid monolayer. Specifically, the phospholipid monolayer promotes alignment of nearby cholesterol esters in a direction normal to the surface, whereas cholesterol esters sitting under ApoB100 tend to align in a direction parallel to the surface. In our two-level system, the average pseudospin,

$$\langle s \rangle = \frac{1}{N} \sum_{\mathbf{i}} s_{\mathbf{i}}, \tag{11}$$

is the coarse-grained analog of the smectic order parameter and we would expect this choice of frozen boundary conditions to induce a similar ordering tendency among spins close to the frozen boundary spins. The calculations described in the previous section may be repeated with this system, and the results for randomly distributed triglyceride defects, shown in Fig. 5, are quite similar to those shown in Fig. 4 which were obtained for periodic boundary conditions.

The nematic order parameter discussed in Ref. [25] carries significantly more information than the pseudomagnetization

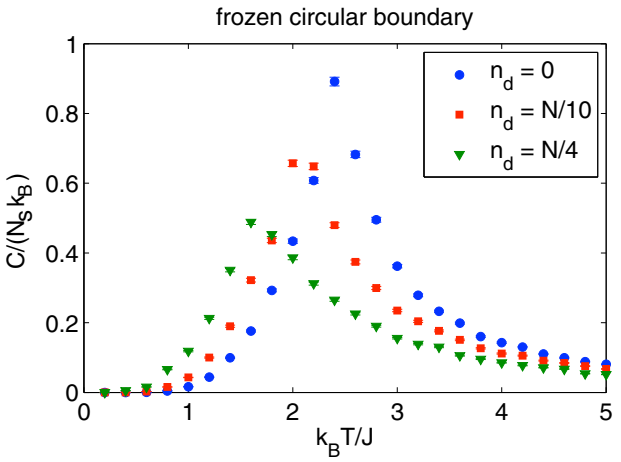

FIG. 5. (Color online) When the domain is taken to be circular with a "frozen" boundary where $s_{\mathbf{i}} = 1$, the results for randomly distributed defects are quite similar to those shown in Fig. 4.

which characterizes order in the Ising model, and the present approach is incapable of distinguishing between the different directions of alignment possible among rod-like cholesterol esters. A potential role that these different types of alignment could play in the overall structure of the core is discussed in Sec. IV C. The main message of this subsection is that choosing boundary conditions in such a way to promote ordering among the spins near the boundary has no significant effect on the nature of the phase transition aside from a very slight broadening of the specific heat curve as can be seen from an examination of Figs. 4 and 5. In other words, at the level of the temperature dependence of the specific heat, the system under consideration is "large enough" to be insensitive to particular details of interactions at the boundary.

Figure 6 demonstrates the system's awareness of the boundary, showing a plot of average magnetization as a function of radial distance from the circular domain's center $(i_x, i_y) = (13,13)$ for a particular temperature $k_B T/J = 2.6$ in the disordered phase for several defect concentrations. The

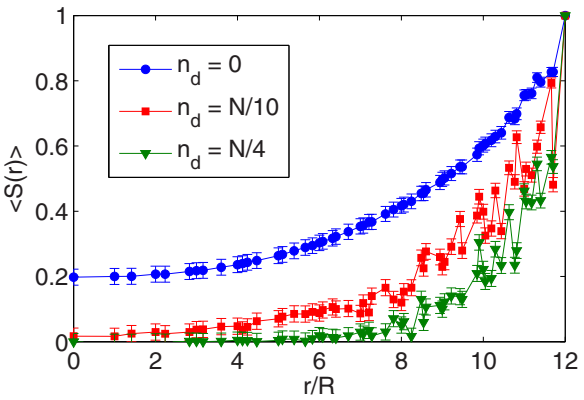

FIG. 6. (Color online) Average magnetization (pseudospin order parameter) as function of distance from the center of the system at a temperature slightly above transition temperature, $k_B T/J = 2.6$. Here $R = 12$ (lattice constants) represents the radial distance of the frozen boundary spins from the center of the system.

magnetization from multiple sites at the same distance from the center was averaged to produce a single value for each radial position (see Appendix A for details). For the case of no defects, the frozen boundary actually induces weak "long-range order" in the finite system which can be seen in Fig. 6 from the decay of the magnetization toward a small but nonzero value in the center of the system. Introducing defects destroys this order in the interior of the system, though the effects of the frozen boundary do remain to some extent close to the edge of the system. It should be noted that the actual critical temperature is different for each defect concentration, and the system with no defects is "closest" to the phase transition of the three systems considered.

Choosing frozen spins or periodic boundary conditions represent only two possibilities for potential boundary conditions. While hardly exhaustive, these two choices represent two somewhat extreme cases, which serve as strong evidence for the robustness of this phase transition with respect to variations in the details at the system boundary. While much has been made of this phase transition in LDL cholesterol, the relatively simple set of ingredients used here suggests this transition should be a generic feature of lipid droplets. Interestingly, a remarkably similar transition has been observed [36] in the lipid droplets within yeast cells. These lipid droplets, with characteristic size $d \approx 400$ nm, are significantly larger than LDL particles and are made of different material. In spite of these vast differences, essentially the same phase transition occurs in both systems, suggesting a simple underlying mechanism such as what we have presented, which makes no reference to the microscopic details of the systems.

IV. ENERGY CONSIDERATIONS: ELASTICITY AND DISTORTIONS

A. Boundary elasticity

In this section, we will attempt to model the effects of a confining lipid-monolayer boundary by treating it as an elastic membrane that surrounds the core lipids within a lipid droplet. As we are employing a liquid-crystal mean-field theory with the aim of qualitative results, we will make several simplifying assumptions along the way to reduce mathematical complications in such a way that has no effect on the general results. The validity of a continuum description is admittedly questionable if quantitative results for small particles such as LDL are to be obtained, and this description is naturally expected to be more reliable with larger particles. However, as the only function of this elastic medium is to provide a mechanism for spherical symmetry to become favorable when interactions between rod-like esters are sufficiently weak, we expect the qualitative picture to remain accurate for smaller particles such as LDL.

A robust model for the distortion energy of a purely elastic membrane is given by the Willmore energy functional from differential geometry [64],

$$W = K_c \int_\Sigma (H^2 - K) dA, \tag{12}$$

where the membrane covers a surface Σ, $H = \frac{1}{2}(\kappa_1 + \kappa_2)$ is the local mean curvature, $K = \kappa_1 \kappa_2$ is the local Gaussian curvature, $\kappa_{1,2}$ are the principal curvatures at a point, and K_c is an elastic modulus giving the integral dimensions of energy. A first variation of the functional yields the nonlinear equation for the extremal surfaces,

$$\nabla^2 H + H(H^2 - K) = 0, \tag{13}$$

whose solutions are known as Willmore surfaces. Often, other terms are introduced to constrain constant volume or surface area or include spontaneous curvature [64]. Such equations can then be used to solve for minimal energy configurations subject to various constraints [65], and at least some analytic solutions are attainable [66]. It should be noted that, in the case of a sphere, the energy W given by Eq. (12) vanishes by virtue of the fact that, for a sphere of radius R, $\kappa_1 = \kappa_2 = R^{-1}$, so that $K = H^2 = R^{-2}$. Thus, any deformation of the shapes of LDL particles from perfect spheres results in an energy penalty given by Eq. (12). Indeed, it should come as no surprise that distortions of the spherical shape of a lipid droplet are highly suppressed, as can be shown by straightforward geometric arguments based on the relevant length scales of the problem [67]. However, as we shall demonstrate in the next two subsections, instabilities can arise when the ordering of structures in the lipid core is also taken into account.

B. Distortions and the smectic phase

The Frank free energy [1] is commonly used as a measure of energy penalties due to distortions in a purely nematic phase,

$$F = \frac{1}{2} \int \{K_1 (\nabla \cdot \hat{n})^2 + K_2 [\hat{n} \cdot (\nabla \times \hat{n})]^2 + K_3 [\hat{n} \times (\nabla \times \hat{n})]^2\} dV, \tag{14}$$

where $|\hat{n}| = 1$, representing the nematic ordering director. The K_i are elastic constants, and the first, second, and third terms (left to right) correspond to "splay," "twist," and "bend" distortions, respectively. Within the smectic phase and under the assumption of an incompressible liquid crystal, the second two distortions are highly suppressed [1]. Thus, the dominant contribution to the distortion energy within the smectic phase is given by the splay term

$$F_0 = \frac{K_1}{2} \int (\nabla \cdot \hat{n})^2 dV. \tag{15}$$

An example of a splay distortion is pictured in Fig. 7. A perfectly ordered smectic phase would correspond to a uniform director field resulting in zero distortion energy. A system with concentric shells, however, would necessarily involve nonzero divergence in the director field, giving rise to a nonzero energy of distortion.

C. Core-ordering instability

In this subsection, we will sketch how competition between the two energy penalties discussed above leads to an instability with respect to purely smectic ordering as the effective interaction between esters is decreased. One can think of increasing triglycerides as a means of "diluting" the esters, resulting in a decreased effective interaction, as discussed in Sec. III.

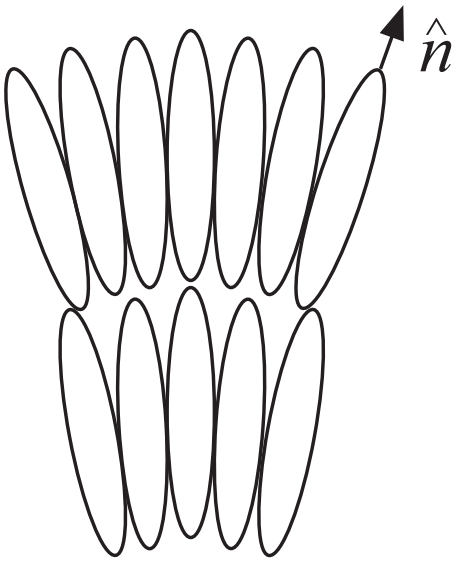

FIG. 7. Schematic of splay distortion in a liquid crystal. The director $\hat{n}$ points parallel to the semimajor axis of the ellipsoidal structures so that physically $\hat{n}$ is equivalent to $-\hat{n}$.

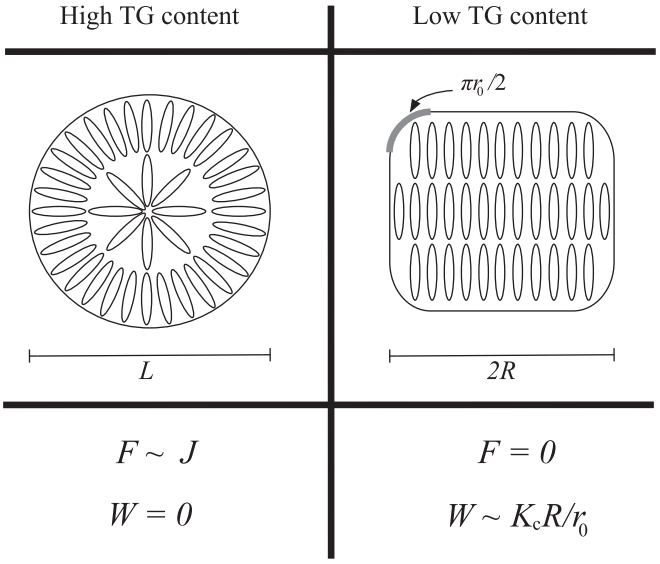

FIG. 8. The role of triglycerides in ordered structures; TG concentration serves as a knob to adjust the effective interactions between the CE molecules.

The splay elastic constant must be proportional to an interaction energy J and has units of energy$\times$ distance^{-1}, so we may write $K_1 = \lambda J/L$, where L is the characteristic size of the LDL particle and λ is a dimensionless constant of order unity. For lamellar structure in the core, we have $\hat{n} \approx \hat{z}$, so that

$$F_{\text{lam.}} \approx 0, \tag{16}$$

whereas for concentric shells of esters in which $\hat{n} = \hat{r}$, where $\hat{r}$ is the unit vector in spherical coordinates, one has $\nabla \cdot \hat{n} = \frac{2}{r}$, so

$$F_{\text{shell}} \approx 8\pi K_1 L \sim J > 0. \tag{17}$$

For a lattice with N spins and zero defects, a fully aligned configuration will have an interaction energy (assuming, without loss in generality, four nearest neighbors)

$$E^{(0)}_{\text{ordered}} = -J \sum_{\langle \mathbf{i},\mathbf{j} \rangle} s_{\mathbf{i}} s_{\mathbf{j}} = -2NJ. \tag{18}$$

If we allow n_d of these lattice sites to contain randomly distributed defects, then there are $N_s = N - n_d$ spins. On average, each spin will have $4\frac{n_d}{N}$ defects as nearest neighbors. The interaction energy of a fully aligned state then becomes

$$E_{\text{ordered}} \approx -\frac{1}{2} J \underbrace{(N - n_d)}_{N_s \text{ spins}} \times \underbrace{4\left(1 - \frac{n_d}{N}\right)}_{\text{n.n. spins}} \tag{19}$$

$$= -2JN_s\left(\frac{1}{\frac{n_d}{N_s} + 1}\right). \tag{20}$$

Thus, a small nonzero fraction of defects modifies the effective interaction J as

$$J_{\text{eff}} \sim J\left(1 - \frac{n_d}{N_s}\right), \tag{21}$$

where n_d is the number of defects, representing triglycerides, and N_{spins} is the number of spins, representing cholesteryl esters. The simple form shown in Eq. (21) can be expected to hold at least for small values of $\frac{n_d}{N_s}$. Figure 8 provides a summary of the distortion energies of the two organizational structures considered. In short, the triglyceride concentration, which modifies the interaction, determines whether elastic deformations of the boundary or splay distortions of the core esters are more energetically costly. A similar situation arises in the Freedericksz transition in nematic liquid crystals [1], in which the liquid crystal director field lowers its energy by aligning with a magnetic field but must exhibit a splay distortion in order to match boundary conditions at hard walls. Below a certain threshold field the distortion penalty outweighs the energetic gain from aligning with the field, and the director field remains uniform. For larger field strengths, the overall energy is lowered in spite of this distortion penalty. The analogy here is that a concentric-shell arrangement of cholesteryl esters can gain energy by rearranging into the lamellar structure described above, but at the cost of warping the surrounding membrane into a nonspherical shape. To fix ideas, let us consider the extreme case by comparing the change in distortion energy of the membrane between the shape of a perfect sphere where $W = 0$ and that of a rounded cylinder, where the flat, circular "caps" are connected to the main "can" of the body by rounded edges of constant curvature radius $r_0 \ll R$, where R is the radius of the cylinder. This smooth boundary represents one half of the outer half of a torus. The geometry is discussed in more detail in Appendix B, and in this limiting case the dominant contribution to the Willmore energy comes from the two smoothed edges, with a contribution

$$W \approx \frac{\pi^2 K_c R}{2r_0}, \tag{22}$$

which diverges in the limit of a kink when $r_0 \to 0$. We note that this divergence is of no practical concern, as it is an artifact of

the continuum description. The smallest radius of curvature r_0 is cut off by the length of a typical phospholipid in the surface layer, which is of comparable size to a typical cholesteryl ester within the lipid droplet. For LDL, this length is of the order $r_0 \sim 3$ nm [40]. The finite sizes of the CE and TG which we have modeled smooth out this divergence which would appear in a strictly continuum description. A rigorous calculation of the surface elastic energy using continuum methods would be dubious for an object as small as an LDL particle, and we simply wish to demonstrate the existence of this surface energy and its role in the competition with the interaction energy which gives rise to core ordering. The evidence for a similar transition taking place in large lipid droplets within yeast cells [36], and the similarities of the core ordering in LDLs to other, larger lipid droplets [37] suggest the basic physics of LDL particles does resemble the physics of larger lipid droplets at the level of detail our analysis is capable of probing. For small particles such as LDL, the limit $r_0 \ll R$ is not necessary valid so that terms of higher order in r_0/R should be included—several of these terms are easily calculated, as shown in Appendix B—or a discrete version of the distortion energy described by Eq. (12) should be employed. The aim here is not a careful calculation of the precise value of this distortion energy but a demonstration that such a nonnegative distortion penalty *exists* for nonspherical surfaces.

Thus, we see that each of the established inner-core structures leads to a particular value for the distortion energy with the spherical shape promoted by concentric shells of the CE resulting in the minimal distortion penalty. Depending on the relative sizes of these energy penalties, one ordered phase will be more stable than the other. In other words, at the current level of detail, a simple picture emerges in which the distortion energy of the system is given by

$$U_{\text{distortion}} \approx \min\left(J, \frac{K_c R}{r_0}\right), \tag{23}$$

with the resulting structure given the configuration shown in Fig. 8 that corresponds to the smallest energy penalty. The main result of this section is that straightforward considerations of distortion energy involved in the two proposed structures for the esters within LD particles suggest triglyceride concentration as an important factor in determining which organization should be present. Both spherical and cylindrical LDL particles have been observed in a large range of particle sizes [40], and high triglyceride content appears to be correlated with spherically shaped particles [68,69], though to date no explanation for this correlation has been proposed. Furthermore, one recent study [35] noted a correlation between low triglyceride levels and lamellar ordering. Our analysis suggests that the triglyceride within lipid droplets content acts as a knob that adjusts the energy penalty associated with spherical ordering, and, in the presence of a large number of triglycerides, the existence of a confining boundary makes the spherical shape energetically favorable compared to the cylindrical shape which allows undistorted smectic ordering of the core lipids.

It is worth noting that a conveniently explicit phenomenology for this structural transition is suggested by the behavior of the nematic order parameter in molecular dynamics computations with LDL. Specifically, cholesterol esters near the phospholipid monolayer tend to align their long axes normal to the surface, which promotes concentric shells of ordered lipids at the cost of a global splay distortion. Should interactions become sufficiently strong by removal of triglycerides this energy penalty can become larger than that required to deform the boundary so that smectic order to be attained by the core lipids. The fact that cholesterol esters tend to align *parallel* to the surface under the ApoB100 protein suggests a mechanism for the symmetry breaking which must occur for the spherically symmetric splay field to break into an axially symmetric arrangement of smectic layers. In this picture, the ApoB100 protein wraps itself around the nematic aligment axis (like a belt), maximizing its contact area with the surface where the ester alignment is parallel to the surface. This picture is consistent with recent high-resolution cryogenic electron microscopy (cryo-EM) reconstructions of the structure of LDL [70], showing a high concentration of rigid protein structures on parts of the surface where the nematic order parameter of the core lipids would indicate parallel aligment with respect the surface.

V. CONCLUSIONS AND DISCUSSION

In this paper, we have presented a simplified framework for describing the phase transition that takes place within the cores of lipid droplets which is based upon the classic Ising model. While the mean-field theory of McMillan [51] often provides an adequate description of the physics of large quantities of cholesteryl esters, a different approach is required for dealing with confined systems. Rather than building a microscopic theory from the ground up, we have employed a coarse-grained approach that, while potentially missing some of the microscopic physics, allows us to study the behavior of a broad class of order-disorder transitions in systems where N is too small for the thermodynamic limit to apply. In this regime, the sharp, double-peaked structure of the specific heat curve in McMillan's theory is blurred into a single rounded peak which washes out the existence of an intermediate nematic phase.

By employing the standard Ising model, which reproduces an effective order-disorder transition in the correct temperature range for the estimated order of magnitude of the interaction energy, we have shown that defects can be used to mimic the effects of triglycerides residing in the core. The defects are assumed to be static, and by changing their distribution from localized to random, we may tune the response of the critical temperature to defect concentration from weak to strong. Unless the defects are given a dynamical degree of freedom and allowed to move through the system, no natural mechanism exists within the current model to provide a crossover between localized TG in the core and randomly distributed TG which serve to dilute the interactions between CE molecules inside the core.

While the crossover behavior occurring at a critical CE/TG ratio of 7:1 lends itself to a simple picture of the core structure in terms of concentric shells of lipids [23], recent compelling evidence has been presented to suggest lamellar ordering of the lipids below the phase transition temperature [22,35,40], at least in some species of LDL. By modeling the effects of a confining lipid monolayer as a simple, elastic membrane, we demonstrate a possible competition in distortion energies

which could be used to tune between the stability of one type of ordering over the other, at least within simple lipid droplets. Recent experiments [68,69], suggest triglyceride content is closely related to the shape of LDL particles, and here we present a possible line of explanation for this correlation in terms of a competition between different distortion energies. Specifically, very high TG content in the core could allow the distortion energy of the membrane to dominate, forcing the particle into a spherical shape instead of the flattened ellipsoid associated with lamellar ordering in the core. It should be noted that, even in experiments where strong evidence was found for this lamellar core ordering, nearly perfectly spherical particles were also observed as a significant fraction of the LDL sample [35,40].

The importance of understanding the order-disorder transition within lipid droplets is twofold: from a physiological standpoint, it would be interesting to determine the biological importance of this transition, if such an importance exists. That the transition occurs so close to biological temperature suggests that individual particles in both phases could potentially exist simultaneously within a single person's LDL population, and understanding whether the core phase dynamically adapts as small temperature changes occur throughout the blood stream could lead to insights regarding the role of LDL in the development of atherosclerosis. Secondly, it is known that an abundance of smaller, denser LDL particles is an atherogenic risk factor [27]. Whether having many smaller LDL particles is an inconsequential effect of another risk factor or itself a cause of atherosclerosis is unknown. Settling this issue through the use of simple, physical models would have drastic implications for the medical community, as LDL particle size is currently used as an assessment of risk without rigorous justification based on the physics of LDL particles. The major conclusion of our present work is that higher triglyceride concentrations might be associated with the more spherically shaped LDL particles, which have a lesser degree of ordering within the core.

Furthermore, if there is something intrinsically damaging or unstable about these smaller particles, there is no physical argument for why this should be so. Our main result is a potential link between lipid droplet core structure and triglyceride concentration. While this in itself admits no simple "cause-and-effect" picture for why smaller LDL particles might be more dangerous than their larger counterparts, our result suggests a physical cause for an instability in triglyceride-rich LDL particles since these cores have a weaker effective interaction energy. Our results are robust in the sense that, by considering a circular domain in which the spins at the edges are all fixed $s_i = 1$, we find a qualitatively similar picture emerge for the behavior of T_c as the defect concentration is varied. This boundary configuration is a crude way of adding a strong tendency of edge particles to order themselves close to the boundary so as to mimic the tendency of cholesteryl esters to align normal to the surface (or parallel to the surface near the ApoB100 protein). That our results survive such perturbations suggest this phase transition is universal in the sense that its presence does not depend on any of the specific details of LDL. This claim is supported by the discovery of a strikingly similar transition within the lipid droplets of yeast cells.

The results of the present work represent a first step toward understanding the physics within the cores of lipid droplets. Significant simplifications of the actual system have been made, and these results need to be taken for what they are; an important step which gives general physical insights and points toward possible directions for future work. Indeed, a common approach in comparably complex systems is the use of molecular dynamics to numerically investigate observables using more microscopically accurate structure and interactions. With such an under-studied system, this type of simulation represents a mammoth task. We are currently pursuing the preliminary stages of such an investigation, and the present work is a preliminary theoretical analysis which provides useful predictions to which future results may be compared. Additionally, with current experiments able to probe the inner core using cryo-EM [22,40] with nearly nanometer resolution, it would be interesting to investigate the details of the core structure as TG concentration in LDLs is varied. Previous studies investigating the dependence of critical temperature on phase transition relied only on small-angle x-ray scattering (SAXS) for inferring any details regarding the structure of the core [23], and later studies of larger yeast cells made identical inferrences based on similar SAXS results [36]. A high-resolution cryo-EM study of these larger yeast cells could shed more light on the possible core structures present in larger lipid droplets. Additionally, such studies could confirm whether the present theoretical picture of the structural crossover being largely dependent on only TG content is sufficient for small particles such as LDL or whether the small size sufficiently impacts the form of the surface distortion energy so that a more complex description is required for understanding the core structure in such droplets.

ACKNOWLEDGMENTS

We thank Dmitry Garanin for helpful discussions.

APPENDIX A: NUMERICAL METHODS

Our results for the specific heat were obtained from Monte Carlo simulations of the Ising model which employ the Metropolis algorithm [54,71] for the approach to thermal equilibrium and generation of states for sampling. In this section, we sketch the details of these computations and our criteria for convergence of the algorithm in the present situation.

The basic problem of statistical mechanics is to calculate observables in a given ensemble. For example, the specific heat of a system can be written

$$C(T) = \frac{\partial}{\partial T}\langle H\rangle = \frac{1}{k_B T^2}(\langle H^2\rangle - \langle H\rangle^2), \qquad \text{(A1)}$$

where H is the Ising Hamiltonian in Eq. (1), and the averages are taken with respect to the canonical ensemble so that the spins may exchange energy with a thermal reservoir. In principle, these averages can be computed by calculating the configuration energy of each microstate. The number of microstates for a square lattice of $n \times n$ spins is 2^N where $N = n^2$, making this entirely unfeasible for all but the smallest systems. The Metropolis algorithm is based on the idea of importance sampling. Most of these microstates have

vanishingly small contributions to observables, and in practice one only needs a sufficiently large subset of microstates relevant to equilibrium states in order to obtain reliable estimates. The first part of the Metropolis prescription is to begin from an arbitrary spin configuration and allow the system to reach thermal equilibrium with its surroundings by flipping single spins,

$$s_{\mathbf{i}} \rightarrow -s_{\mathbf{i}}, \tag{A2}$$

for some spin $\mathbf{i} = (i_x, i_y)$ in the square lattice. If this change results in a decrease of the system's energy, it is accepted. If the change raises the system's energy, it is accepted with probability $p = e^{-\Delta E/(k_B T)}$, where ΔE is the change in energy caused by the single spin flip. Thus process is repeated many times, allowing the system to thermalize [71]. The sites are chosen randomly, and each spin is allowed to change its orientation about once every N steps on average for a system of N spins. A sequence of N steps constitutes one "sweep" of the system and provides a metric for relaxation time which is independent of system size [71].

After reaching thermal equilibrium, the system is sampled, generating states which fluctuate in energy around the equilibrium average $\overline{E} = \langle H \rangle$. These microstates generated after equilibration provide a large sample of states with significant Boltzmann weights which can be used to estimate observables.

In first set of calculations (see Figs. 3–4), we take the system to be a 20×20 square lattice of 400 spins. Generally speaking, error can arise either from not allowing the system to approach thermal equilibrium and from not allowing enough sampling steps for the sum to converge to the true average. We first address the issue of approaching thermal equilibrium. Essentially, we must make sure that the average energy saturates to some constant when averaged over a moving window during the sampling. To avoid mistaking a metastable state for equilibrium, we observe the average energy for two extreme cases of the initial configuration. Namely, we repeat the calculation for a fully ordered initial configuration (all spins equal to, say, 1) and a completely random initial configuration. These configurations correspond to a zero-temperature equilibrium state and an infinite-temperature equilibrium state, respectively. Thus, to ensure the system has relaxed sufficiently, we continue sweeping until both states relax to states of equal average energy.

As an example of the metastable states which arise when considering systems with zero-spin defects, consider a random distribution of defects. Figure 9 shows configuration energy as a function of sweep number for a defect density of $x = n_d/N = 0.2$, where N is the total number of lattice sites and n_d is the number of defect cells. In this regime, the high-temperature initial state takes much longer to fully relax than the zero-temperature initial state. The reason for this long thermalization time is shown in Fig. 10. With a sufficient number of defects, domain walls are much less energetically offensive when they follow the defect distribution. Because of this enhanced stability of domain walls, the thermalization time is significantly enhanced. This enhancement is not present in the basic Ising model or in the case with localized defects. After a sufficiently large number of sweeps, the disordered state eventually thermalizes, attaining the same average energy as the initially ordered system does, in the sense of a moving-

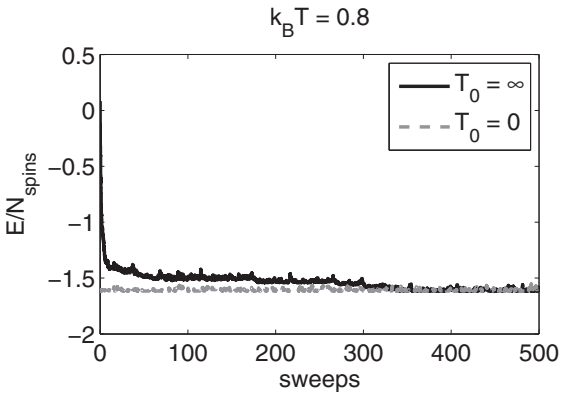

FIG. 9. Individual configuration energy plotted versus number of sweeps of the Metropolis algorithm for the infinite (solid black line) and zero (dashed grey line) temperature initial states. The high-temperature initial conditions lead to a long-lived metastable state, which is reached after about 100 sweeps. This metastable state eventually decays after about 350 sweeps.

window average. One could make the valid point that waiting for a system initially held at infinite temperature to cool to very low temperatures is a rather inefficient route, and in this situation the low-temperature initial conditions should be used. Our point of view is that by allowing both extreme cases sufficient time to converge to the same state, we remove any reasonable doubt of being in the genuine equilibrium state for further sampling. With the modest system sizes investigated in this paper, such brute-force calculations are hardly intractable. We found 15 000 system sweeps to be adequate for complete relaxation of the inifinite-temperature initial configuration except for several isolated cases where twice this number of sweeps was necessary.

The second source of error is statistical in nature. After the system reaches equilibrium, we must sample enough states so that the Monte Carlo average,

$$\overline{A} \equiv \frac{1}{n} \sum_j A_j, \tag{A3}$$

converges to the true system average

$$\langle A \rangle = \frac{1}{Z} \sum_{\text{states } s} A(s) e^{-\beta E(s)}. \tag{A4}$$

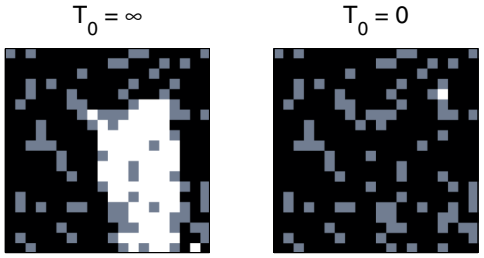

FIG. 10. (Color online) Spin configurations after 250 Metropolis sweeps of the different initial conditions for $k_B T$ below the critical temperature. Black (white) cells correspond to a spin value of -1 ($+1$), and the defect cells are grey. The ratio of defects to total lattice sites is 0.2.

When measuring local observables such as the magnetization, a good estimate for the uncertainity δA is the standard deviation [71]

$$\delta A \approx \sigma_A \approx \sqrt{\frac{2\tau}{N_{\text{sweeps}}}(\langle A^2\rangle - \langle A\rangle^2)}, \tag{A5}$$

which is valid when the time between measurements is significantly shorter than the system's correlation time $\Delta t \ll \tau$, where τ is conveniently defined by the autocorrelation function for the observable A,

$$\chi_A(t) = \int dt'[\langle A(t')A(t'+t)\rangle - \langle A\rangle^2] \sim e^{-t/\tau} \tag{A6}$$

The error bars in Fig. 6 were thus computed according to Eq. (A5) using τ obtained from a fitting of the magnetization autocorrelation function to an exponential function. For the temperature considered ($\frac{T-T_c}{T_c} \simeq 0.15$) we find $\tau \simeq 25$ sweeps, so $\tau = 50$ sweeps was used as a conservative estimate. Sampling was performed at a rate of about one sample per system sweep so $\Delta t = 1$ sweep, satisfying $\Delta t \ll \tau$. For the purpose of studying how the critical temperature varies, we are not interested in high-precision estimates for individual values of $C(T)$, and we have chosen N_{sweeps} large enough to obtain qualitatively accurate trends for $C(T)$, as shown by the relatively small error estimates depicted in Figs. 3 and 4. As a measurement of $C(T)$ itself is a measure of fluctuations of the energy, a bootstrap resampling [71] was necessary to obtain the error estimates depicted in Figs. 3–5.

The simulations thus consist of the following steps: for a fixed value of the temperature, the Metropolis algorithm is employed with the change in energy for a single spin flip $\Delta s_{\mathbf{i}}$ given by

$$\Delta E = -J\Delta s_{\mathbf{i}} \sum_{\mathbf{j}=\text{n.n.}} s_{\mathbf{j}}, \tag{A7}$$

where "n.n." stands for "nearest neighbors" of the site $\mathbf{i}$. This is repeated until the initially random and initially ordered configurations yield the same average energy, signaling that the system has truly equilibrated. The specific heat depends upon $\langle H^2\rangle$ and $\langle H\rangle$, which are computed by recording the values of H and H^2 after each sweep following equilibration. Sufficient convergence of the statistical averages is obtained by performing an additional 4×10^4 sweeps for sampling, as indicated by the error bars in Figs. 3 and 4.

When the circular boundary is employed (see Figs. 5–6) the procedure just outlined is only slightly altered. Namely, only sites living within the domain $\mathcal{D}$ defined in Eq. (10) are sampled or used as possible sites for defects, so these are the only sites which contribute to the interaction energy of the system. The behavior of the specific heat curve is rather insensitive to this change in boundary conditions (cf. Figs. 4 and 5), and we demonstrate the nonvanishing effects of the boundary by showing the averaged spin for the clean system (no defects) as a function of distance from the domain's center. The average is taken with respect to Monte Carlo samplings at individual sites. Figure 6 shows these spin averages as a function of a single distance r, where

$$r = \sqrt{\left(i_x - \frac{n}{2}\right)^2 + \left(i_y - \frac{n}{2}\right)^2}. \tag{A8}$$

In general, there are multiple sites $\mathbf{i} = (i_x, i_y)$ which correspond to the same value of r, so the values $\langle S(r)\rangle$ depicted in Fig. 6 represent an average over these multiple sites yielding a single averaged spin value for each radial distance r.

APPENDIX B: CURVATURE OF A ROUNDED CYLINDER

In Sec. IV, we made use of the curvature of a torus and integrated this across a quarter of the toroidal surface. Here we justify the expression used there. A torus may be written as a surface in three-dimensional space parameterized by the angles θ and ϕ as

$$x = (R_t + r_0\cos\theta)\cos\phi, \tag{B1}$$

$$y = (R_t + r_0\cos\theta)\sin\phi, \tag{B2}$$

$$z = r_0\sin\theta. \tag{B3}$$

We use R_t to distinguish this length from the effective radius of the actual cylinder, $R = R_t + 2r_0$. One can immediately read off the principal radii of curvature, the reciprocals of which give the principal curvatures,

$$\kappa_1 = \frac{1}{r_0}, \tag{B4}$$

$$\kappa_2 = \frac{1}{R_t + r_0\cos\theta}. \tag{B5}$$

The Willmore energy is then given by

$$W_{\text{torus}} = \frac{K_c}{4}\int_\Sigma (\kappa_1 - \kappa_2)^2 dA \tag{B6}$$

$$= \frac{\pi^2 K_c}{4}\left(\frac{R_t}{r_0}\right) + \frac{\pi K_c}{2}(1-\pi) + \frac{\pi r_0 K_c}{R_t}\frac{\tan^{-1}\left[\sqrt{\frac{1-\frac{r_0}{R_t}}{1+\frac{r_0}{R_t}}}\right]}{\sqrt{1-\left(\frac{r_0}{R_t}\right)^2}} \tag{B7}$$

$$\xrightarrow{r_0 \ll R_t} \frac{\pi^2 K_c R_t}{4r_0}. \tag{B8}$$

Each "cap" of the cylinder gives rise to a contribution to the Willmore energy given by Eq. (B8). Additionally, there is a contribution from the rounded body of the cylinder,

$$W_{\text{cylinder}} = K_c\int (H^2) dA \tag{B9}$$

$$= \frac{\pi K_c h}{2R}, \tag{B10}$$

where h is the height of the cylinder. For lipid droplets $h \sim R$, and this is negligible compared to Eq. (B8) when $r_0 \ll R \approx R_t$. Thus, the leading term in the Willmore energy comes from the rounded edges and is given by

$$W_{\text{total}} = \frac{\pi^2 K_c R}{2r_0}. \tag{B11}$$

[1] P. M. Chaikin and T. C. Lubensky, *Principles of Condensed Matter Physics* (Cambridge University Press, Cambridge, UK, 1995).

[2] J. P. Sethna, *Statistical Mechanics: Entropy, Order Parameters and Complexity* (Oxford University Press, Oxford, England, 2006).

[3] T. L. Hill, *Thermodynamics of Small Systems* (W. A. Benjamin, New York, 1963).

[4] *Heat Capacities: Liquids, Solutions and Vapors*, edited by E. Wilhelm and T. Lechter (Royal Society of Chemistry, Cambridge, UK, 2010).

[5] N. Krahmer, Y. Guo, R. V. Farese, Jr., and T. C. Walther, Cell **139**, 1024 (2009).

[6] H. Yang, A. Galea, V. Sytnyk, and M. Crossley, Curr. Opin. Cell Biol. **24**, 509 (2012).

[7] D. L. Brasaemle, J. Lipid Res. **48**, 2547 (2007).

[8] M. Beller, K. Thiel, P. J. Thul, and H. Jäckle, FEBS Lett. **584**, 2176 (2010).

[9] M. Digel, R. Ehehalt, and J. Füllekrug, FEBS Lett. **584**, 2168 (2010).

[10] S. Martin and R. G. Parton, Sem. Cell Dev. Biol. **16**, 163 (2005).

[11] D. J. Murphy, Prog. Lipid Res. **40**, 325 (2001).

[12] T. C. Walther and R. V. Farese, Jr., Biochim. Biophys. Acta **1791**, 459 (2009).

[13] M. A. Welte, Trends Cell Biol. **17**, 363 (2007).

[14] A. S. Greenberg, R. A. Coleman, F. B. Kraemer, J. L. McManaman, M. S. Obin, V. Puri, Q.-W. Yan, H.i Miyoshi, and D. G. Mashek, J. Clin. Invest. **121**, 2102 (2011).

[15] W. S. Blaner, S. M. O'Byrne, N. Wongsiriroj, J. Kluwe, D. M. D'Ambrosio, H. Jiang, R. F. Schwabe, E. M. C. Hillman, R. Piantedosi, and J. Libien, Biochim. Biophys. Acta **1791**, 467 (2009).

[16] D. A. Brown, Curr. Biol. **11**, R446 (2001).

[17] J. S. Alpert, Am. J. Med. **125**, 839 (2012).

[18] R. Prassl and P. Laggner, in *Lipoproteins - Role In Health and Diseases*, edited by S. Frank and G. Kostner (InTech, Rijeka, Croatia, 2012).

[19] M. Suzuki, Y. Shinohara, Y. Ohsaki, and T. Fujimoto, J. Electron Microsc. (Tokyo) **60** (Suppl. 1), S101 (2011).

[20] R. J. Deckelbaum, G. G. Shipley, and D. M. Small, J. Biol. Chem. **252**, 744 (1977).

[21] R. J. Deckelbaum, G. G. Shipley, D. M. Small, R. S. Lees, and P. K. George, Science **190**, 392 (1975).

[22] Y. Liu, D. Luo, and D. Atkinson, J. Lipid Res. **52**, 256 (2011).

[23] M. Pregetter, R. Prassl, B. Schuster, M. Kriechbaum, F. Nigon, J. Chapman, and P. Laggner, J. Biol. Chem. **274**, 1334 (1999).

[24] T. Hevonoja, M. O. Pentikäinen, M. T. Hyvonen, P. T. Kövanen, and M. Ala-Korpela, Biochim. Biophy. Acta **1488**, 189 (2000).

[25] T. Murtola, T. A. Vuorela, M. T. Hyvönen, S.-J. Marrink, M. Karttunen, and I. Vattulainen, Soft Matter **7**, 8135 (2011).

[26] S. Le Lay and I. Dugail, Prog. Lipid Res. **48**, 191 (2009).

[27] M. Rizzo and K. Berneis, QJM **99**, 1 (2006).

[28] A. S. Greenberg and M. S. Obin, Cell Metab. **7**, 472 (2008).

[29] S. Martin and R. G. Parton, Nat. Rev. Mol. Biol. **7**, 373 (2006).

[30] D. J. Murphy and J. Vance, Trends Biol. Sci. **24**, 109 (1999).

[31] C. Thiele and J. Spandl, Curr. Opinion Cell Biol. **20**, 378 (2008).

[32] R. V. Farese, Jr. and T. C. Walther, Cell **139**, 855 (2009).

[33] S. Murphy, S. Martin, and R. G. Parton, Biochim. Biophys. Acta **1791**, 441 (2009).

[34] H. Robenek, I. Buers, O. Hofnagel, M. J. Robenek, D. Troyer, and N. J. Severs, Biochim. Biophys. Acta **1791**, 408 (2009).

[35] G. Ren, G. Rudenko, S. J. Ludtke, J. Deisenhofer, W. Chiu, and H. J. Pownall, Proc. Natl. Acad. Sci. USA **107**, 1059 (2010).

[36] T. Czabany, A. Wagner, D. Zweytick, K. Lohner, E. Leitner, E. Ingolic, and G. Daum, J. Biol. Chem. **283**, 17065 (2008).

[37] M. J. Robenek, N. J. Severs, K. Schlattmann, G. Plenz, K.-P. Zimmer, D. Troyer, and H. Robenek, FASEB J. **18**, 866 (2004).

[38] B. Schuster, R. Prassl, F. Nigon, M. J. Chapman, and P. Laggner, Proc. Natl. Acad. Sci. USA **92**, 2509 (1995).

[39] D. Atkinson, R. J. Deckelbaum, D. M. Small, and G. G. Shipley, Proc. Natl. Acad. Sci. USA **74**, 1042 (1977).

[40] E. V. Orlova, M. B. Sherman, W. Chiu, H. Mowri, L. C. Smith and A. M. Gotto, Jr., Proc. Natl. Acad. Sci. USA **96**, 8420 (1999).

[41] R. V. Antwerpen and J. C. Gilkey, J. Lipid Res. **35**, 2223 (1994).

[42] J. R. McNamara, D. M. Small, Z. Li, and E. J. Schaefer, J. Lipid Res. **37**, 1924 (1996).

[43] K. K. Berneis and R. M. Krauss, J. Lipid Res. **43**, 1363 (2002).

[44] R. E. Morton and J. S. Parks, J. Lipid Res. **37**, 1915 (1996).

[45] R. Zechner, G. M. Kostner, H. Dieplinger, G. Degovics, and P. Laggner, Chem. Phys. Lipids **36**, 111 (1984).

[46] J. E. Roeters van Lennep, H. T. Westerveld, D. W. Erkelens, and E. E. van der Wall, Cardiovasc. Res. **53**, 538 (2002).

[47] J. A. Houmard, N. J. Bruno, R. K. Bruner, M. R. McCammon, R. G. Israel, and H. A. Barakat, Arterioscl. Thromb. **14**, 325 (1994).

[48] H. Esterbauer, M. Dieber-Rotheneder, G. Waeg, G. Striegl, and G. Jürgens, Chem. Res. Toxicol. **3**, 77 (1990).

[49] C. Packard, M. Caslake, and J. Shepherd, Int. J. Cardiol. **74**, S17 (2000).

[50] K. Skøalén, M. Gustafsson, E. K. Rydberg, L. M. Hultén, O. Wiklund, T. L. Innerarity, and J. Borén, Nat. Lett. **417**, 750 (2002).

[51] W. McMillan, Phys. Rev. A **4**, 1238 (1971).

[52] W. Maier and A. Saupe, Z. Naturforsch. **13a**, 564 (1958); **14a**, 882 (1959); **15a**, 287 (1960).

[53] C. Burks and D. M. Engelman, Proc. Natl. Acad. Sci. USA **78**, 6863 (1981).

[54] H. Gould and J. Tobochnik, *Statistical and Thermal Physics with Computer Applications* (Princeton University Press, Princeton, NJ, 2010).

[55] L. Onsager, Phys. Rev. **65**, 117 (1944).

[56] E. Agliari, A. Barra, A. Galluzzi, A. A. Pizzoferrato, and D. Tantari, *Mathematical Models and Methods for Planet Earth*, Springer INdAM Series, edited by A. Celleti, U. Locatelli, T. Ruggeri, and E. Strickland (Springer, New York, 2014), Vol. 6, pp. 73–86.

[57] D. A. Pink, C. B. Hanna, C. Sandt, A. J. MacDonald, R. MacEachern, R. Corkery, and D. Rosseau, J. Chem. Phys. **132**, 054502 (2010).

[58] S. Doniach, J. Chem. Phys. **68**, 4912 (1978).

[59] P. A. Lebwohl and G. Lasher, Phys. Rev. A **6**, 426 (1972).

[60] M. E. Fisher and H. Au-Yang, J. Phys. C: Solid State Phys. **8**, L418 (1975).

[61] A. Labarta, J. Marro, B. Martinez, and J. Tejada, Phys. Rev. B **38**, 500 (1988).

[62] P. L. Garrido and J. Marro, J. Phys. A: Math. Gen. **25**, 1453 (1992).

[63] D. Stauffer, Phys. Rep. **54**, 1 (1979).

[64] W. Helfrich, Z. Naturforsch. **28c**, 693 (1973).

[65] O.-Y. Zhong-can and W. Helfrich, Phys. Rev. Lett. **59**, 2486 (1987).
[66] H. Naito, M. Okuda and O.-Y. Zhong-can, Phys. Rev. E **48**, 2304 (1993).
[67] A. Penno, G. Hackenbroich, and C. Thiele, Biochim. Biophys. Acta. **1831**, 589 (2013).
[68] M. B. Sherman, E. V. Orlova, G. L. Decker, W. Chiu, and H. J. Pownall, Biochemistry **42**, 14988 (2003).
[69] A. Coronado-Gray and R. van Antwerpen, Lipids **40**, 495 (2005).
[70] V. Kumar, S. J. Butcher, K. Öörni, P. Engelhardt, J. Heikkonen, K. Kaski, M. Ala-Korpela, and P. T. Kovanen, PloS ONE **6**, e18841 (2011).
[71] M. E. J. Newman and G. T. Barkema, *Monte Carlo Methods in Statistical Physics* (Oxford University Press, Oxford, England, 1999).